Laser-induced incandescence particle image velocimetry (LII-PIV) for simultaneous two-phase flame velocity measurement

Luming Fan[a], Cheng Tung Chong[b,c,*], Bo Tian[a], Yutao Zheng[a], Dante McGrath[a], Simone Hochgreb[a]

[a] *Hopkinson Laboratory, Department of Engineering, University of Cambridge, Trumpington Street, CB2 1PZ, United Kingdom*
[b] *China-UK Low Carbon College, Shanghai Jiao Tong University, 201306 Lingang, Shanghai, China*
[c] *School of Mechanical Engineering, Faculty of Engineering, Universiti Teknologi Malaysia, 81310, Skudai, Johor, Malaysia*

Abstract

In a previous study we demonstrated a novel two-phase PIV technique based on the laser-induced incandescence (LII) signal from black submicron tungsten carbide particles (WC), which achieved velocity measurement for both dispersed-form (large water droplet) and continuous-form (gas). Submicron WC particles are intentionally seeded into a two-phase flow, and heated by a light sheet generated by a double-pulsed PIV laser running at high energy. The 200 nm diameter, light absorbing WC particles are heated to several thousand degrees to emit strong incandescence signals, whilst the temperature rise in liquid droplets or large particles remains negligible. The small particles follow the gas phase flow, unlike the droplets which may have a different velocity. Droplets are detected via the Mie scatter signal at the same incident wavelength, whereas the LII signal from small WC particles is detected

*Corresponding author:
Email address: ctchong@sjtu.edu.cn (Cheng Tung Chong)

Preprint submitted to Proceedings of the Combustion Institute, 38

at a suitably different wavelength within the LII emission spectrum, thus allowing discrimination of velocities between phases. The LII-PIV technique had been implemented with a low-speed CCD PIV camera in non-reacting flows. In flames, the strong flame luminosity saturated the second frame due to the long exposure time as the characteristics of the device. To solve this problem, in the present study, we synchronized two high-speed CMOS cameras to a low speed laser. One records the LII signal and the other records the Mie scatter signal from 36.6 μm water droplets. The scattering from WC particles appears only as a weak background signal in the Mie image, which can be easily removed by applying a high-pass filter. Simultaneous velocity measurements for both gas and liquid phase are demonstrated in an air jet, a cold impinging flow, and finally in a Bunsen flame. The last two cases are repeated using the traditional two-phase PIV technique based on image segmentation so as to conduct a fair comparison of both techniques. We show that LII-PIV can achieve the same level of accuracy as the segmentation method in non-reacting flows, and can be applied to measure in flames with two-phase flows with less stringent requirements regarding seeding quality.

Keywords: LII-PIV, two-phase PIV, tungsten carbide, slip velocity, Bunsen flame

---

1. Introduction

Two-phase flames are of wide interest since many engines and combustors are based on combustion of fuel spray or solids. In practical applications, these droplets or solids range from tens to hundreds micrometers, and are often injected with high momentum. Their motion can be quite different from the gaseous flow in which they are oxidised. Gravity and initial momentum together determine the residence time of the particles in the reaction zone, and for volatile fuel droplets in particular, the slip motion also affects the evaporation rate [1, 2]. Therefore, a velocimetry technique that can resolve the motion of both dispersed phase and continuous phase is necessary. For this purpose, the flow diagnostics community has introduced several two-phase PIV techniques. Based on the strategy used, there are two possible categories: a two-color method and an image segmentation method. The two-color method uses fluorescent particles to separate the Mie scatter signal from large droplets, for example [3, 4]. This method is not significantly limited by the droplet density, but the fluorescent dopant decomposes in a flame, or produces very low signal yield at high temperatures, hence is not suitable for flame studies. The image segmentation technique uses Mie scatter images from both large droplets and micron-sized particles acquired with one single camera, which are then separated by applying a complex image processing algorithm based on the intensity differences [5], particle image size [6], shape [7], or their combinations [8]. The image segmentation method has many limitations regarding the dynamic range of droplet size and droplet number density, and has not yet been applied to flames.

In a previous study [9], we demonstrated the use of laser-induced incandescence (LII) signal from black submicron particles, rather than fluorescence, to perform two-color PIV in a cold droplet-laden flow. These black tracers were heated to several

thousand degrees to emit strong incandescence signal by a double-pulsed PIV laser operating at sufficiently high energy, whilst the laser-induced temperature rise in large droplets or solids was negligible. By recording the LII signal at a wavelength different from Mie scattering, the motion of the black tracers, which represented the gaseous flow field, was successfully separated from the dispersed phase (ethanol droplets) [9]. For reacting flows, we proposed to use tungsten carbide (WC) particles to serve as the tracer, since they have large absorption efficiency for laser light and can sustain extremely high temperatures up to 3000 K. Calculations showed that a common PIV seeding rate of 10^{11} particles/m^3 led to negligible laser heating effect on local gas temperature, and so did the radiative heat loss due to the particle glow [9]. WC particles can be slowly oxidised into WO_2 and WO_3 after firing at high temperatures for several hours [10]. Comparing with the short chemical reaction time scale of methane at adiabatic temperature (several microseconds) and the kinetic time scale of flames (ranges from hundreds microseconds to milliseconds typically), the oxidation of WC is too slow and should have little effect on the flame.

However, a problem was identified when conducting LII-PIV in flames using a low-speed CCD double-frame camera: the second frame was saturated by flame luminosity due to its long exposure time (∼150 ms), which could not be controlled. Since LII signal bursts and quickly decays within microseconds after the laser pulse, one straightforward solution is to reduce the shutter time to gate out flame luminosity. In that work [9], we suggested to use an extra shutter to reduce the exposure time for the second frame, or to add more cameras to capture the second pulse separately, or to use high-speed cameras which have much shorter shutter time for both frames when operating at high frequencies.

In the present study, we chose the last solution and synchronized two high-speed CMOS cameras with a low frequency laser (10 Hz) to realise LII-PIV in a two-phase

flame. High frequency lasers usually do not have sufficient output energy to form a reasonably large light sheet that can heat the particles to LII temperatures, so a high-energy but low-frequency laser was used. The cameras were running in PIV mode at 5 kHz so as to achieve a shutter time of 100 μs for each frame. Empty images were discarded, and image recording was repeated multiple times to collect a sufficient number of images for each test condition. Simultaneous two-phase velocity measurements were conducted in an air jet, a cold impinging flow, and finally in a Bunsen flame, all laden with 36.6 μm mean diameter water droplets generated by a Sono-Tek ultrasonic atomizer. To make a back-to-back comparison with the image segmentation technique, we repeated the impinging flow and the Bunsen flame case using that method. The advantages and limitations of the two techniques for both non-reacting and reacting flows are reported.

2. Experimental setup

2.1. Flow configuration and PIV tracers

Figure 1 illustrates the experimental setup. A laminar flame burner was used to produce the air jet, cold impinging flow (with a plate) and the Bunsen flame described in the following sections. The burner consists of a 70 mm inner diameter chamber, with a height of 260 mm which converges to an aerodynamically shaped nozzle of 14 mm exit diameter shrouded by a 9 mm wide annular nitrogen co-flow. A Sono-Tek (120-1009) ultrasonic atomizer was used to generate large water droplets with a size distribution from 20 to 60 μm, as shown in Fig. 2(a), which was measured by a Dantec phase Doppler anemometer at 1 mm above the burner exit. The arithmetic mean diameter is 36.6 μm and SMD is 40.7 μm. These water droplets served as the dispersed phase in all the following cases. The main advantages of using this

ultrasonic atomizer over the previous air-blasting one [9] are that it does not produce high intensity noise that can cause flame instability, and that the droplet size distribution is relatively compact. This facilitates the image segmentation method, which has significant limitations on the dynamic range of droplet size. Water was injected into the atomizer by a syringe pump. Not all water droplets can reach the burner exit, hence calibration tests were conducted to quantify the water trapped inside the burner after running the two-phase flow for a long time. We estimated that only 60% of injected water left the burner. Water flow rates mentioned in this paper are values obtained after correction.

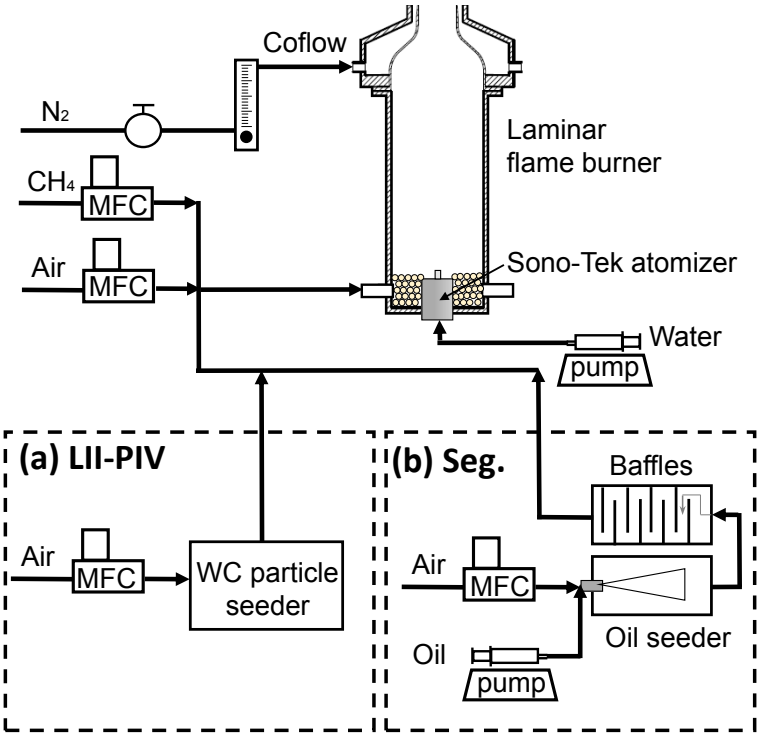

Figure 1: Schematic of the burner and atomizing system, and tracer delivery system for (a) LII-PIV, and (b) image segmentation method.

For LII-PIV, WC particles (WC02N, A.L.M.T.) as in [9] were used as the tracer

for the gaseous flow. The primary particle has a 0.2 μm SMD (reported by the supplier), but they form 1-2 μm small clusters as shown in the Scanning Electron Microscope (SEM) image in Fig. 2(b). For the image segmentation method, vegetable oil droplets were produced by an air-blasting atomizer and served as the gas flow tracer. The carrier gas together with the oil droplets was forced to pass through an impactor chamber, which consisted of several baffles. Any large oil droplets that cannot follow the sharp velocity gradient would be stopped by the baffles and stay inside the chamber. The mean oil droplet size measured at the burner exit is 1.7 μm, with a maximum of roughly 5 μm. The size distribution of the oil droplets are also plotted in Fig. 2(a).

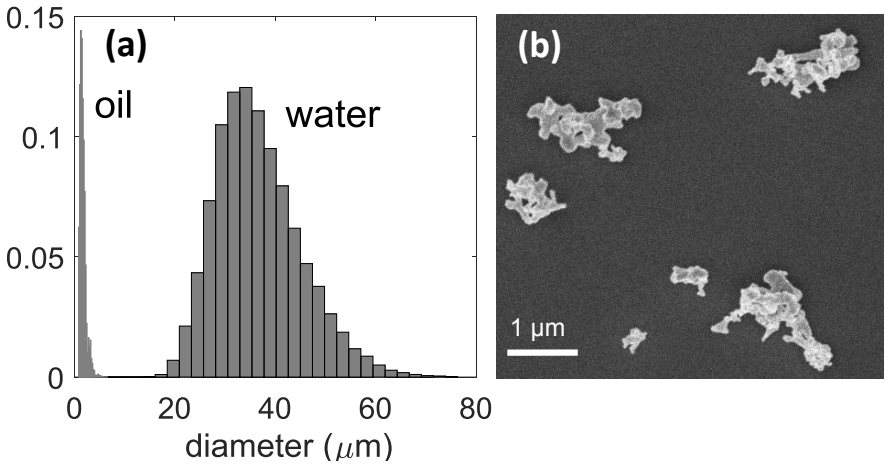

Figure 2: (a) PDFs of water and oil droplet size distribution measured by PDA; (b) SEM image of the tungsten carbide sample (WC02N).

2.2. Optical setup for LII-PIV

Two CMOS cameras (Phantom V611) were separately used to record the Mie scatter signal from water droplets and the LII signal from WC particles. They were synchronized with a low-speed Litron Nano-PIV laser. The cameras were operated

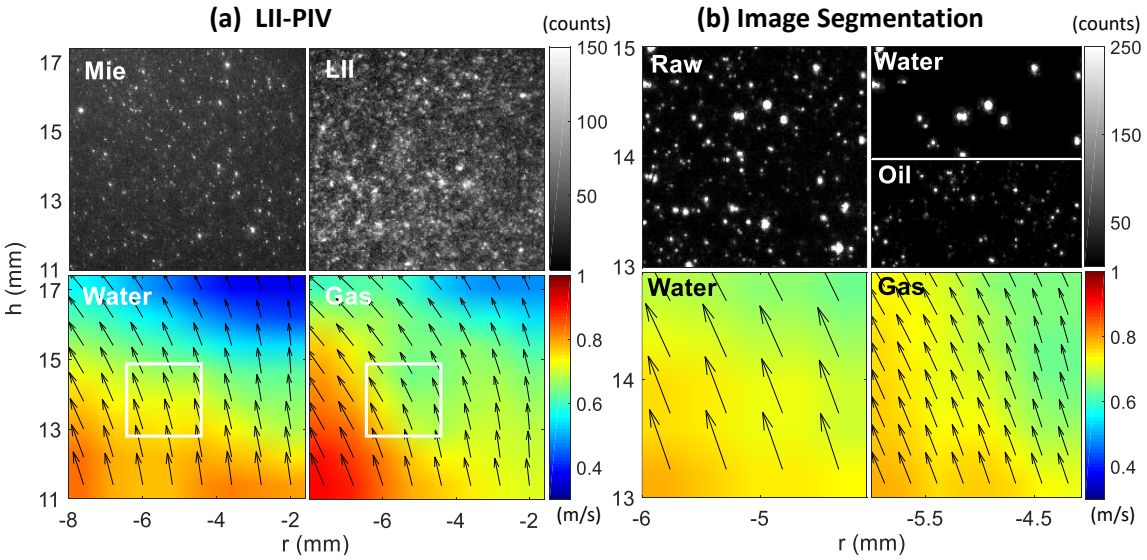

Figure 3: Example raw PIV images top (an impinging flow) and the resulting simultaneous gas and water velocity fields (bottom) for (a) LII-PIV and (b) image segmentation method over a 200 × 200 pixel field. The white squares in (a) mark the relative position of (b). Missing vectors in (b) due to sparse seeding were filled by interpolation.

at 5 kHz in double frame mode whilst the double-pulsed laser was triggered at 10 Hz. A total of 10000 image pairs were recorded each time by each camera, only 20 of which (1 out of 500) were with signals and saved, in synchronization with the laser pulses. The exposure time for each frame was 100 μs. Image acquisition was repeated 10 times for each condition to collect 200 samples. Since recording 10000 images only takes 2 seconds, the data collection process was still efficient and did not take a long time compared with the low-speed system.

The laser beam was expanded to form a light sheet. The side-wings along both vertical and out-of-plane direction of the Gaussian laser profile were trimmed by a slit to create a top-hat intensity profile. A convex lens of focal length 500 mm was set after the slit to narrow down the laser sheet. Finally, a 22 mm in height and 0.5 mm thick laser sheet with a uniform fluence distribution was formed at the test

field. The laser energy at the test section was measured as 60 mJ for both pulses. A Nikkor 50 mm Microlens was combined with a Sigma × 2 teleconverter to focus the camera on the measurement plane. Because of the high framing rate used, the frame size was reduced to 640 × 800 pixels to measure a test field of about 2.1 × 2.6 cm^2. The resolution was 32.3 and 30.1 μm/pixel for the Mie and LII cameras, respectively. Image mapping and scaling were conducted using a purpose-built target from La Vision.

The Mie scatter camera was installed with a 532 ± 1.5 nm filter to remove background noise. A neutral density filter of power 2 was also added, and the lens aperture was reduced to $f/D = 8$ to avoid damage to the camera. On the other side, the LII camera was installed with a 425 ± 25 nm filter, and the aperture was wide open (f/D=1.4) to guarantee a robust LII signal.

2.3. Optical setup for image segmentation method

The laser alignment was kept unchanged, but the energy was adjusted to 5 mJ for both pulses. The laser fluence was uniformly distributed in the illumination volume, therefore the brightness and shape of droplet images had a strong correlation with the droplet size primarily, rather than its location. A CCD camera (Lavision Imager ProX) was operated at 5 Hz to record the Mie signal from both water and oil droplets. The image segmentation method requires very high spatial resolution, so that all oil and water droplets are sparsely distributed on the image and can be easily separated. The combination of a Nikkor 60 mm Microlens and the Sigma teleconverter was used, and the final pixel resolution was calibrated as 10.2 μm/pixel. Since the CCD camera sensor has 2048×2048 pixels (2.1×2.1 cm^2), the full image field extends to the CMOS camera image width, with a shorter height. A 532 ± 1.5 nm filter and an aperture size of f/D = 5.6 was set to guarantee a sufficient signal from oil droplets, but at

the same time to avoid sensor damage by the strong scattering from water droplets.

3. Data processing

Figure 3(a) shows the raw Mie scattering and the LII image of a non-reacting mixture, and the corresponding vector fields. In the Mie image, there is a weak background signal at about 20-30 counts, probably due to the Mie scattering from small particles or multiple scattering. Hence, a high-pass filter was applied to remove the sliding background at a length scale larger than 15 pixels. The water spots range from 4 to 10 pixels with a peak intensity from several hundreds to a maximum about 2000 counts. For the LII images, particle image patterns can be seen clearly and all LII signals arise due to the WC particles, hence no image pre-processing was conducted. A 32×32 interrogation window was used for both water and gas velocity. Vectors with a Q-factor less than 1.2 were removed.

For the image segmentation method, a size threshold (a median filter at 8 pixels) was combined with an intensity threshold at 800 counts to create a *mask* to separate the oil and water droplet images. After image segmentation, a 64×64/32×32 window size was used to calculate the vector field of water/gas, respectively. The 1.2 Q-factor criterion was also applied to remove spurious vectors. Fig. 3(b) shows an example PIV image for both water and oil droplets, the (upper half) images after segmentation, and the resulting velocity field for each phase. To maximize the detectablity of small and large droplet images, the spatial resolution for this technique needs to be very high, whilst the seeding density should be relatively low. This raises two issues for further consideration: firstly, the extent of the field of view is sacrificed for achieving a high spatial resolution. This suggests the segmentation method is good for identifying individual droplets, whilst LII-PIV is suitable for observing larger flow structures with lower spatial resolution. This is illustrated by the white square

in Fig. 3(a) which marks the relative position of Fig. 3(b) for a same sensor area (200×200 pixels); secondly, the segmentation method requires a careful optimization between sufficient seeding for high quality PIV measurement, and the ease to separate large and small particles. In this study, missing vectors due to sparse seeding were filled by interpolation. For the laminar flame used in this study, interpolation does not result in significant bias because the velocity field is expected to be very smooth.

4. Demonstration of LII-PIV in a two-phase air jet

In previous work [9], we measured the gas-phase and liquid-phase velocities non-simultaneously by deploying different filters to a single low-speed PIV camera. In this section, we demonstrate *simultaneous* measurement of velocity fields for both gas and liquid phase in an air jet using LII-PIV with the two CMOS cameras. The same burner was used to generate an air jet flow, with 2.4 m/s bulk flow velocity (20 slpm) and Re = 2200 at room temperature. The water flow rate was 0.9 mL/min. Figure 4 presents an example of Mie and LII images recorded simultaneously, and the corresponding velocity field for water and gaseous flow. Since the unprocessed Mie image contains a weak background signal from WC particles, it can be observed that the water droplets appear to be less involved into the entrainment structures marked by the WC particles. The velocity fields of liquid phase and gas phase show a similar structure, as shown in figure 4 (bottom row). ~~, except that the gas velocity field appears to be wavier.~~

Figure 5 shows the mean and RMS velocity field for water droplets and the gaseous flow, respectively. The axial slip velocity between two phases is not as evident as in our previous findings [9]. This may be explained by the higher outlet velocity and a smaller nozzle (14 mm) used in the current test, which provided a

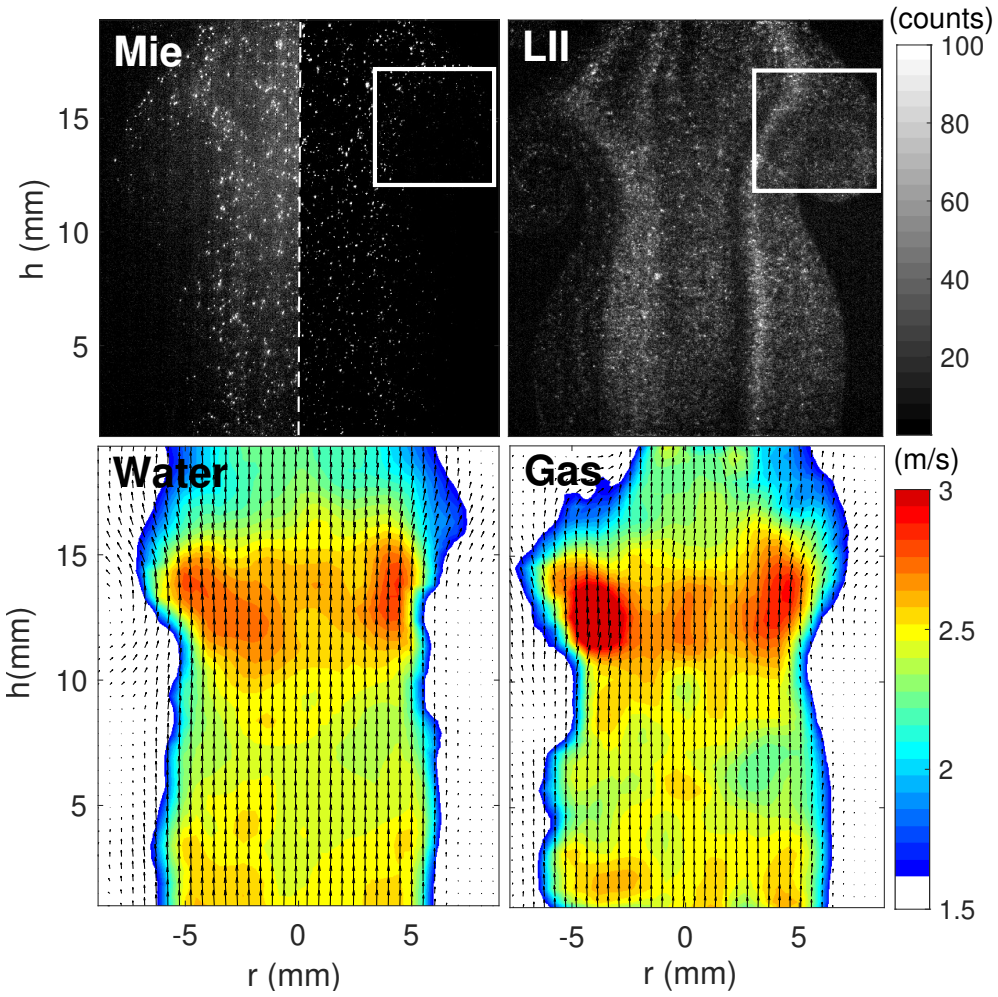

Figure 4: Simultaneous water and gaseous flow velocity measurement using LII-PIV for a Re = 2200 air jet. Top images: the left half of the Mie image shows the unprocessed raw image, in which a low level background Mie signal from WC particles can be observed, whilst the right half was processed by a high-pass filter. An entrainment structure is highlighted by a white square on both channels. Bottom images: 2D velocities, with vector length marked in colour map.

higher acceleration effect on the droplets. The height of measurement field (20 mm from the nozzle exit) was also much shorter than the previous experiment (60 mm), so the effect of gravity is not as apparent. ~~Given their slow response to the ambient flow conditions,~~ Water droplets show a lower velocity RMS in the shear layer above 10 mm, where the vortical structures have fully developed. This is expected, since large water droplets have slow response to the fluctuation of gaseous flow in the shear layer, where the Stokes number for water droplets is estimated as about 3 (thus too slow to follow the flow fluctuations), whilst the corresponding number for WC particles is of order 0.03, and follows the gas flows. A further reason is the lower signal which arises from the entrainment of unseeded co-flow, which reduces the number of particles in each interrogation window, compared with the water droplets which do not mix as fast.

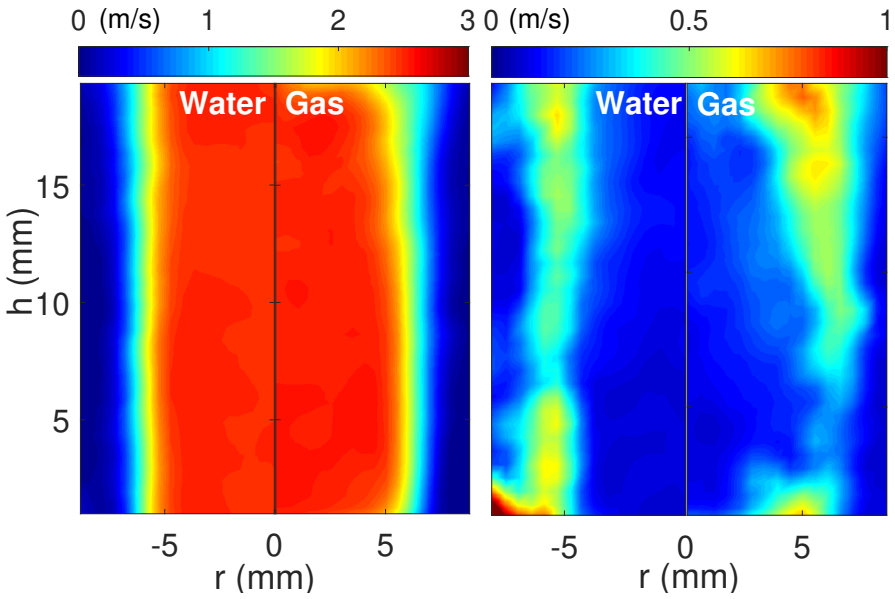

Figure 5: (*left*) Mean velocity and (*right*) RMS for water droplets and gaseous flow in the air jet case. Statistics are calculated based on 200 single shots.

5. Non-reacting two-phase impinging flow

In order to reveal the slip motion of large droplets, we replaced the 14 mm burner nozzle with a 22 mm diameter unit used in the previous study, and added an impinging surface 20 mm above the nozzle to intentionally exert a strong pressure gradient. The air flow rate was 25 slpm, corresponding to a 1.2 m/s bulk velocity at the burner exit. The strain rate for this case is estimated as 90 s^{-1}, which is proportional to the flow deceleration. Water droplets were dispersed into the flow for a 1.1 mL/min liquid flow rate. Both LII-PIV and image segmentation method were applied and the resulting velocity fields are presented and compared in Fig. 6.

The mean axial velocity profiles measured by the two methods agree very well for both gaseous and liquid phase. A 0.1 m/s initial slip velocity can be identified at the burner exit, as the converging nozzle cannot accelerate the large droplets as quickly as the gaseous flow. Once leaving the burner, the flow starts to decelerate as it approaches the impinging surface. Again, the large droplets show a slow response to the pressure gradient, and produce a relative slip velocity of 0.07 m/s at $y = 15$ mm. In the image segmentation method, the field of view was sacrificed for gaining higher spatial resolution, thus the height of the image field ends 17 mm above the nozzle. Both CCD and CMOS camera images start from 3 mm upstream of the nozzle. The velocity RMS obtained from the segmentation method (error bars) is higher than that from the LII-PIV method (shaded area), especially for the liquid phase. This is attributed to the relative high noise in the velocity measurement led by low particle image density. Of course, the precision of the segmentation method could be improved further by optimizing the seeding rate. The impinging flow result shows that the performance of the LII-PIV technique is as good as the conventional image segmentation method in non-reacting flows.

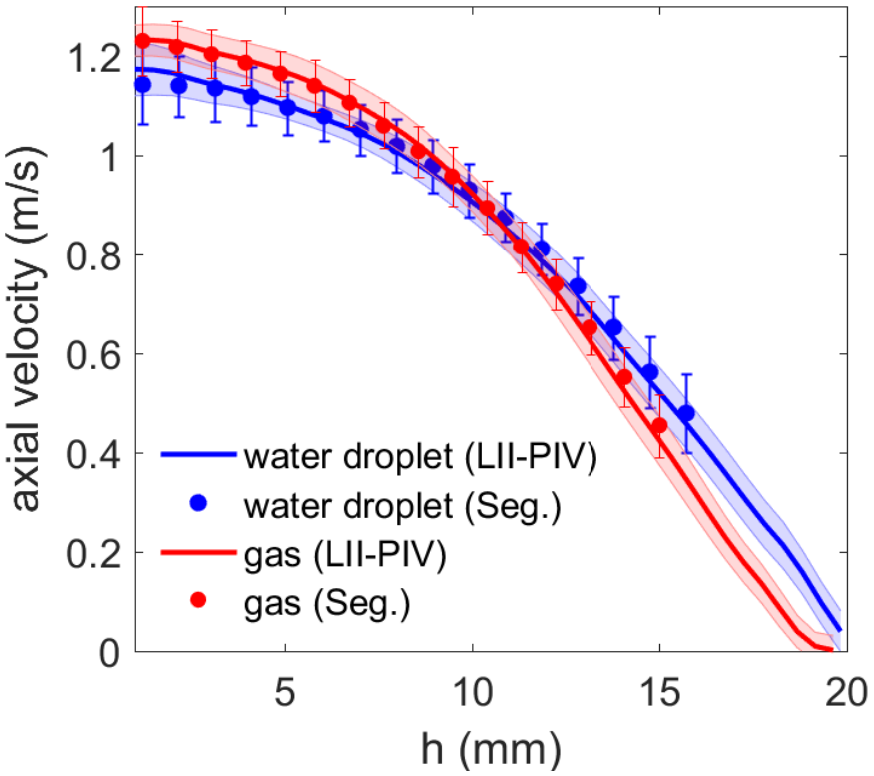

Figure 6: Comparison of LII-PIV and image segmentation method in a two-phase impinging flow at 25 slpm and 20 mm nozzle-plate distance. The centre-line axial velocity profile is extracted and averaged over 200 single shots. The RMS velocity is shown as shaded area or as error bars. For a better display of results, the velocity profile based on image segmentation is down-sampled and plotted as solid circles.

6. Bunsen flame laden with water droplets

In the previous study [9], the attempt to apply LII-PIV to a stagnation flame was not successful, as the second frame of the low speed camera was saturated by the flame luminosity, due to the long exposure time ($\sim$ 150 ms) and the wide bandwidth of the LII filter. In the current setup, the shutter time for the CMOS cameras is 100 μs for each frame. In theory, the recorded flame luminosity is now reduced by a factor of 10^{-4}. For this demonstration, the 14 mm converging nozzle was used. Methane/air/water mixture at an equivalence ratio of 1.1 was ignited and

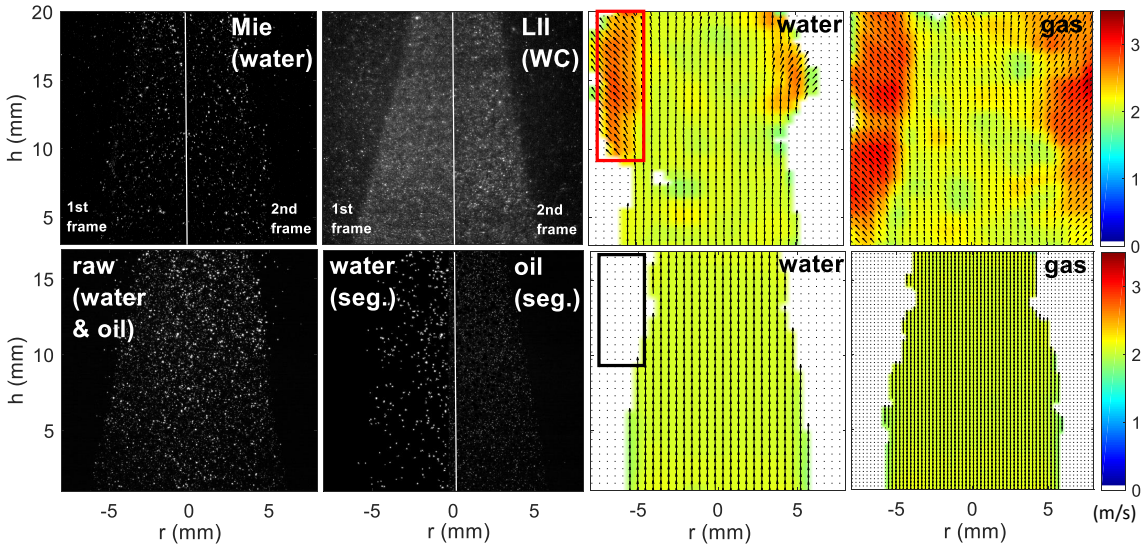

Figure 7: Simultaneous single-shot velocity measurements for both gas and liquid phase in a Bunsen flame laden with water droplets, using (*upper row*) the LII-PIV technique and (*bottom row*) the image segmentation method with oil droplets, respectively. The red rectangle marks a product region where droplet velocity was resolved by LII-PIV, but not by the image segmentation method (black rectangle).

stabilized to form a Bunsen flame at a bulk flow rate of 18 slpm. The water flow rate was 0.9 mL/min. Fig. 7 shows the result of simultaneous velocity measurement for both water and gas, using LII-PIV (*upper row*) and the image segmentation method (*bottom row*). With the high-speed CMOS cameras, frames of the LII image were not saturated, and thus can be used for cross-correlation. Unlike oil or water droplets, WC particles can survive in the flame, hence the gas flow velocity field in the whole area was resolved, including the product region. The image segmentation method with oil, however, only measured the velocity field in the unreacted region. In the past, the velocity measurements in the product region of a single-phase flame were achieved by using solid tracers such as alumina or titania particles. However, Fig.8 shows a problem arising from applying these seeding methods to a two-phase flame: the particle seeder used cannot keep a truly constant seeding rate, which is a common

challenge for most solid particle seeding devices, so the data quality for segmentation varies from shot to shot. Here we have two sample images extracted from the same dataset at the same condition as in Fig. 7, but now with alumina particles as the gas tracer. In Fig. 8(a) the seeding rate was low and could be used for segmentation, whereas in (b) the water droplet images were entirely submerged into the alumina particle images and could not be separated by any image processing tool. Therefore, in absence of a stable seeding device for solid tracers, the LII method offers significant advantages relatively to the segmentation method for reacting flows, because it can spectrally separate the signal from gas and liquid phases and thus does not pose strict requirements on the seeding quality. Nevertheless, we note that if stable seeding can be achieved, the image segmentation method could also be applied to flames with similar performance.

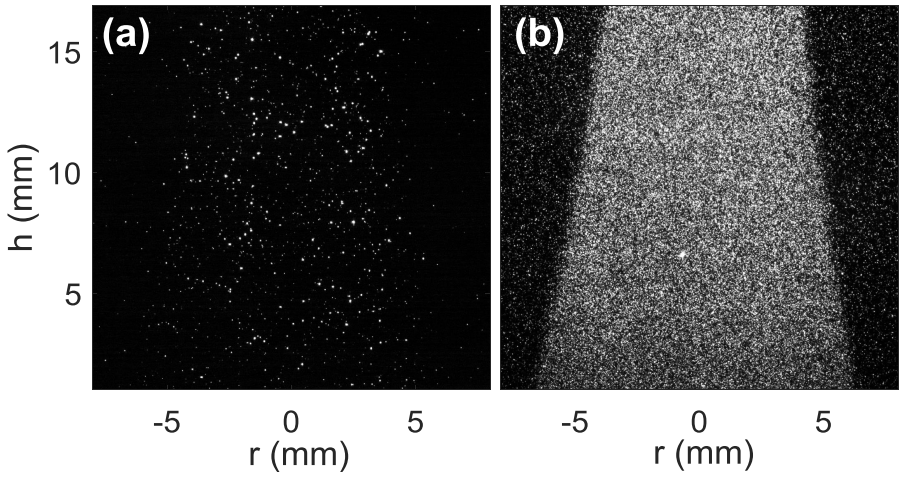

Figure 8: Image segmentation method with alumina tracers at (a) low and (b) high seeding rate, respectively. The two images were extracted from the same dataset, but the seeding rate was not consistent in time.

Figure 7 also shows how a few water droplets can penetrate the flame front and enter the reaction zone over a short distance. Vectors of the liquid phase beyond

the flame front were resolved by the LII-PIV technique, as highlighted by the red rectangle in Fig. 7. However, this event is not captured in the result obtained by the image segmentation method (see the black rectangle marking the same region). Because the droplet size and brightness decreases quickly once entering the flame front, the water droplet images in the reaction zone were filtered out by the intensity and size thresholds during the image processing. In principle, this could be solved by adopting an adaptive threshold along the droplet trajectory, which remains an interesting topic for future studies on the application of segmentation method on two-phase flames, or on volatile fuel droplets. Nevertheless, the insensitivity to seeding suggests a good suitability of the LII-PIV technique in such reacting flows.

7. Conclusions

The use of LII-PIV using 200 nm diameter WC particles as the gas tracer was successfully demonstrated to measure velocity fields for both dispersed and continuous phase simultaneously in a two-phase flow/flame laden with water droplets. The flame luminosity problem reported in the previous study was solved by using two CMOS high-speed cameras running at 5 kHz to record the two wavelengths (532 nm and 425 nm, respectively). This two-color approach allows the discrimination of the droplets relatively to particles in simultaneous shots, and opens the way for characterizing slip velocities between droplets and surrounding gases in more complex flows.

The method was then compared to the currently established image segmentation method for the same test cases in non-reacting and reacting flows. The results show that the LII-PIV method has very good agreement with the segmentation method in non-reacting flows, and offers the advantage of enabling the measurements in product zones. The price of the LII-PIV technique is the need to seed the flow

with WC (which is not onerous), and the need for sufficient laser energies to induce incandescence in those small black particles. The minimum laser fluence for signal is estimated as 0.4 J/cm^2 for the WC particles and laser wavelength used in this study.

In the present case high-speed PIV cameras were use in combination with a lower frequency, higher pulse energy laser to allow visualisation of a sensible field of view. It would of course be possible to generate high speed LII-PIV if the laser pulses have sufficient energies for LII. Conversely, a low-speed PIV camera enabled with suitably short shuttering capabilities for the second frame would also be suitable.

Finally, we anticipate that the overall method could also be useful in other flow situations whenever particles of tens to hundreds micrometers are involved, such as coal and metal particles.

Acknowledgments

The authors gratefully acknowledge the financial support from Newton Advanced Fellowship (NA160115). Additional funding was provided by a subcontract from Universiti Teknologi Malaysia. The authors also acknowledge Dr. Xiao Zhang for conducting the SEM tests, and A.L.M.T. Corp (Japan) for providing tungsten carbide samples and relevant data.

References

[1] J. B. Greenberg, Finite-rate evaporation and droplet drag effects in spherical flame front propagation through a liquid fuel mist, Combustion and Flame 148 (2007) 187–197.

[2] A. L. Sánchez, J. Urzay, A. Liñán, The role of separation of scales in the

description of spray combustion, Proceedings of the Combustion Institute 35 (2015) 1549–1577.

[3] D. P. Towers, C. E. Towers, C. H. Buckberry, M. Reeves, A colour PIV system employing fluorescent particles for two-phase flow measurements, Measurement Science and Technology 10 (1999) 824–830.

[4] K. D. Driscoll, V. Sick, C. Gray, Simultaneous air/fuel-phase PIV measurements in a dense fuel spray, Experiments in Fluids 35 (2003) 112–115.

[5] J. Sakakibara, R. B. Wicker, J. K. Eaton, Measurements of the particle-fluid velocity correlation and the extra dissipation in a round jet, International Journal of Multiphase Flow 22 (1996) 863–881.

[6] Y. A. Hassan, T. K. Blanchat, C. H. Seeley, R. E. Canaan, Simultaneous velocity measurements of both components of a two-phase flow using particle image velocimetry, International Journal of Multiphase Flow 18 (1992) 371–395.

[7] K. T. Kiger, C. Pan, PIV Technique for the Simultaneous Measurement of Dilute Two-Phase Flows, Journal of Fluids Engineering 122 (2000) 811.

[8] D. A. Khalitov, E. K. Longmire, Simultaneous two-phase PIV by two-parameter phase discrimination, Experiments in Fluids 32 (2002) 252–268.

[9] L. Fan, D. McGrath, C. T. Chong, M. N. Mohd Jaafar, H. Zhong, S. Hochgreb, Laser-induced incandescence particle image velocimetry (LII-PIV) for two-phase flow velocity measurement, Experiments in Fluids 59 (2018) 156.

[10] A. S. Kurlov, A. I. Gusev, Oxidation of tungsten carbide powders in air, International Journal of Refractory Metals and Hard Materials 41 (2013) 300–307.